

Relativistic effective interaction for nuclei, giant resonances, and neutron stars

F. J. Fattoyev,^{1,*} C. J. Horowitz,^{2,†} J. Piekarewicz,^{1,‡} and G. Shen^{2,§}

¹*Department of Physics, Florida State University, Tallahassee, FL 32306*

²*Nuclear Theory Center and Dept. of Physics, Indiana University, Bloomington, IN 47405*

(Dated: August 19, 2010)

Nuclear effective interactions are useful tools in astrophysical applications especially if one can guide the extrapolations to the extremes regions of isospin and density that are required to simulate dense, neutron-rich systems. Isospin extrapolations may be constrained in the laboratory by measuring the neutron skin thickness of a heavy nucleus, such as ^{208}Pb . Similarly, future observations of massive neutron stars will constrain the extrapolations to the high-density domain. In this contribution we introduce a new relativistic effective interaction that is simultaneously constrained by the properties of finite nuclei, their collective excitations, and neutron-star properties. By adjusting two of the empirical parameters of the theory, one can efficiently tune the neutron skin thickness of ^{208}Pb and the maximum neutron star mass. We illustrate this procedure in response to the recent interpretation of X-ray observations by Steiner, Lattimer, and Brown that suggests that the *FSUGold* effective interaction predicts neutron star radii that are too large and a maximum stellar mass that is too small. The new effective interaction is fitted to a neutron skin thickness in ^{208}Pb of only $R_n - R_p = 0.16$ fm and a moderately large maximum neutron star mass of $1.94 M_\odot$.

PACS numbers: 26.60.Kp, 21.65.Cd, 21.60.Jz

I. INTRODUCTION

Nuclear effective interactions provide a compact and efficient description of both the structure of finite nuclei and the equation of state—pressure as a function of density and temperature—of nuclear matter. Effective interactions are often fitted to well determined nuclear observables, such as binding energies and charge radii of closed shell nuclei. However, limiting the calibration procedure to these few properties leaves important parts of the effective interaction largely undetermined, particularly the isovector interaction. Failure to constrain the isovector interaction affects the properties of systems with large isospin asymmetry. In the case of finite nuclei, perhaps the best example is the neutron radius (or neutron skin) of heavy nuclei. Indeed, effective interactions calibrated to the binding energy and charge radii of closed-shell nuclei often predict significantly different neutron radii [1, 2]. In the case of infinite matter, it is the density dependence of the symmetry energy that remains largely unconstrained. These poorly constrained properties are very important in astrophysical systems with large neutron asymmetries, such as neutron stars [3–8].

In this article we develop an effective interaction suitable for the calculation of the ground-state properties of finite nuclei, their collective response, and the structure of neutron stars. Astrophysical predictions are notoriously difficult as they involve two large extrapolations away from the familiar landscape of stable nuclei. Whereas one involves isospin extrapolations from the domain of stable nuclei to the very neutron-rich systems present in neutron stars, the other one involves an extrapolation from the density of normal nuclei to the very high (and very low) densities that are encountered in neutron stars. To reduce the uncertainties associated with these extrapolations we impose two additional constraints—one experimental and one observational—on the effective interaction. Specifically, we extend the standard protocol of fitting to the binding energies and charge radii of finite nuclei by demanding that the new effective interaction also reproduces: (a) the neutron radius of ^{208}Pb and (b) the maximum mass of a neutron star. We have selected these two quantities over other possible choices because they can be determined in a model independent manner from experiment and observation. In particular, fixing the neutron radius in ^{208}Pb reduces significantly the uncertainties associated with extrapolations in isospin. The Lead Radius experiment (PREx)—which was successfully commissioned in March of 2010—aims to determine the neutron radius of ^{208}Pb in a model independent fashion by using parity violating electron scattering [9, 10]. To reduce the uncertainty associated with extrapolations to high

*Electronic address: ff07@fsu.edu

†Electronic address: horowit@indiana.edu

‡Electronic address: jpiekarewicz@fsu.edu

§Electronic address: gshen@indiana.edu

densities, we have selected to fix the maximum neutron star mass. Of course, the maximum neutron star mass selected for the fit must at least be equal to the largest—well measured—mass determined from observation [11].

In principle, other choices are possible to guide these extrapolations. For example, laboratory experiments with heavy ions have played a critical role in probing the nuclear equation of state. By tuning the energy of the colliding beams and the neutron-proton asymmetry, heavy-ion collisions probe vast regions of the phase diagram. In particular, isospin diffusion data may be used to constrain the density dependence of the symmetry energy [12–14]. This could be used instead of the neutron radius in ^{208}Pb . Moreover, experiments with very energetic heavy ions have compressed nuclear matter to densities in excess of four times nuclear matter saturation density [15]. The determination of the pressure of symmetric nuclear matter at these high densities may be used instead of the maximum neutron star mass. However, not only is the interpretation of heavy-ion data model dependent, but heavy-ion systems are much less neutron rich and often much hotter than neutron stars. This introduces large and uncontrolled uncertainties.

Neutron star radii as a function of mass—the so-called *Mass-vs-Radius* relationship—provides critical information on the equation of state of neutron-rich matter at high densities. Yet, the simultaneous determination of both the mass and radius of a neutron star is difficult. However, tremendous advances in X-ray astronomy have produced large amounts of high quality data that have allowed the simultaneous determination of both masses, radii, and the underlying equation of state [16, 17]. Unfortunately, neutron star radii inferred from X-ray observations of the luminosity and temperature are sensitive to models of the stellar atmosphere (see Ref. [18] and references therein). Moreover, mass and radius determination from X-ray burst (as in Ref. [16]) may be hindered by systematic uncertainties [17]. For example Ozel, Baym, and Güver inferred very small stellar radii from their recent analysis of three X-ray bursts [16], while Steiner, Lattimer, and Brown extracted neutron star radii significantly larger (of the order of 12 km) [17]. Still, we believe that such studies will eventually become instrumental in constraining the dense matter equation of state.

In the past, we have studied correlation between the neutron skin of ^{208}Pb and the non-uniform solid crust of a neutron star [3]. For models with a stiff equation of state, namely, one where the pressure increases rapidly with density, it is energetically unfavorable to separate uniform nuclear matter into regions of high and low densities. Thus, models with a stiff equation of state predict low transition densities from non-uniform to uniform neutron-rich matter. The neutron skin thickness in ^{208}Pb also depends on the equation of state of neutron-rich matter: the stiffer the equation of state the thicker the neutron skin. Thus, an inverse relationship was established: *the thicker the neutron skin of a heavy nucleus, the lower the transition from non-uniform to uniform neutron-rich matter*. This represents one of the many examples that show the utility of constraining the neutron skin thickness in ^{208}Pb —and consequently the effective interaction—for astrophysical applications.

Many relativistic effective interactions exist. For example, the NL3 interaction [19, 20] provides an excellent description of the binding energy and charge radii of many nuclei throughout the periodic table. When extrapolated to the neutron-star domain, the NL3 effective interaction predicts a very stiff equation of state that generates both large stellar radii and a large maximum neutron star mass. On the other hand, the FSUGold (or FSU for short) interaction [21] also provides a good description of closed shell nuclei, but predicts a significantly softer equation of state. Indeed, whereas NL3 predicts a maximum neutron star mass of $2.78 M_\odot$, the FSU interaction predicts a limiting mass almost one full solar mass smaller (of $1.72 M_\odot$). The softer equation of state emerges as one incorporates constraints from giant resonances and heavy-ion collisions. At present, we are not aware of any nuclear effective interaction that also incorporates astrophysical constraints in the calibration procedure. It is the aim of the present manuscript to obtain a new effective interaction that improves on both NL3 and FSU by incorporating some of the recent constraints suggested by Steiner, Lattimer, and Brown [17]. In particular, we will show that the EOS predicted by the new model generates a limiting neutron star mass intermediate between NL3 and FSU but stellar radii smaller than both.

We have organized our article as follows. In Section II we describe details of the fitting procedure and present results for several ground-state properties of closed shell nuclei. Next, we show in Section III how the new effective interaction reproduces the properties of various nuclear collective modes. Predictions for the equation of state and for various properties of neutron stars are presented in Section IV. Finally, we conclude in Section V.

II. RELATIVISTIC EFFECTIVE FIELD THEORY

Our starting point will be the relativistic effective-field theory of Ref. [22] supplemented with an isoscalar-isovector coupling as introduced in Ref. [3]. The interacting Lagrangian density for this model is given by [3, 22]

$$\begin{aligned} \mathcal{L}_{\text{int}} = & \bar{\psi} \left[g_s \phi - \left(g_v V_\mu + \frac{g_\rho}{2} \boldsymbol{\tau} \cdot \mathbf{b}_\mu + \frac{e}{2} (1 + \tau_3) A_\mu \right) \gamma^\mu \right] \psi \\ & - \frac{\kappa}{3!} (g_s \phi)^3 - \frac{\lambda}{4!} (g_s \phi)^4 + \frac{\zeta}{4!} g_v^4 (V_\mu V^\mu)^2 + \Lambda_v g_\rho^2 \mathbf{b}_\mu \cdot \mathbf{b}^\mu g_v^2 V_\nu V^\nu. \end{aligned} \quad (1)$$

The model contains an isodoublet nucleon field (ψ) interacting via the exchange of two isoscalar mesons, the scalar sigma (ϕ) and the vector omega (V^μ), one isovector meson, the rho (\mathbf{b}^μ), and the photon (A^μ). In addition to meson-nucleon interactions, the Lagrangian density includes scalar and vector self-interactions. (Note that while the original model allows for ρ -meson self-interactions [22], their phenomenological impact has been documented to be small so they will not be considered in this contribution). The scalar self-interaction is responsible for reducing the compression modulus of nuclear matter from the unrealistically large value of $K=545$ MeV [23, 24] all the way down to about $K=230$ MeV. This latter value appears to be consistent with measurements of the isoscalar giant monopole resonance (GMR) in ^{208}Pb [25–28].

Omega-meson self-interactions, as described by the parameter ζ , soften the equation of state at high density and can be tuned to reproduce the maximum mass of a neutron star. Indeed, Müller and Serot found it was possible to build models with different values of ζ that reproduce the same observed properties at normal nuclear densities, yet produced maximum neutron star masses that differ by almost one solar mass [22]. In particular, models with $\zeta=0$ predict large limiting masses of about $2.8M_\odot$ —even for models with a soft symmetry energy. In contrast, the nonlinear coupling constant Λ_v was included to modify the density-dependence of the symmetry energy. Tuning Λ_v provides a simple and efficient method of softening the symmetry energy without compromising the success of the model in reproducing well determined ground-state observables [21]. Here we will adjust Λ_v by assuming a relatively small value for the neutron skin thickness of ^{208}Pb . Many properties of finite nuclei, such as the binding energies and charge radii of closed shell nuclei, are insensitive to the values of ζ and Λ_v . Indeed, the NL3 effective interaction reproduces these observables without ever introducing these two empirical parameters. Our approach here is to accommodate newly proposed astrophysical constraints that suggest that, relative to the FSU interaction, the equation of state of stellar matter must be slightly softer at intermediate densities and stiffer at high densities [17].

The new effective interaction is generated by adopting the following procedure. We start from the FSU parameter set [21] as listed in Table I. This parameter set reproduces ground-state properties and collective excitations of closed shell nuclei. However, this interaction has a relatively large value of $\zeta = 0.06$. This reduces the pressure at high densities and generates a relatively small neutron star maximum mass of $1.72 M_\odot$. Note that, to date, the only terrestrial constraint on the high-density component of the EOS comes from energetic heavy-ion collisions [15]. The FSU equation of state fits these data comfortable within the errors. Yet, the reported errors are large enough to accommodate slightly stiffer equations of state. As we aim for an interaction with a somewhat larger maximum mass of about $2.0 M_\odot$, we reduce the value of ζ from 0.06 to 0.03. Next, we refit the isoscalar parameters (g_s , g_v , κ , and λ) to maintain the saturation properties of symmetric nuclear matter at their FSU values, namely, a saturation density of 0.148 fm^{-3} (or a Fermi momentum of $k_F = 1.30 \text{ fm}^{-1}$), an energy per nucleon of $E/A = -16.30 \text{ MeV}$, and an incompressibility coefficient of $K=230 \text{ MeV}$.

Model	m_s	m_v	m_ρ	g_s^2	g_v^2	g_ρ^2	κ	λ	ζ	Λ_v
NL3	508.194	782.501	763.000	104.3871	165.5854	79.6000	3.8599	-0.015905	0.00	0.000
FSU	491.500	782.500	763.000	112.1996	204.5469	138.4701	1.4203	+0.023762	0.06	0.030
IU-FSU	491.500	782.500	763.000	99.4266	169.8349	184.6877	3.3808	+0.000296	0.03	0.046

TABLE I: Parameter sets for the three models discussed in the text. The parameter κ and the meson masses m_s , m_v , and m_ρ are all given in MeV. The nucleon mass has been fixed at $M=939 \text{ MeV}$ in all the models.

We then increase the isoscalar-isovector coupling constant Λ_v from its FSU value of 0.03 to 0.046. This change softens the density dependence of the symmetry energy and reduces the neutron radius in ^{208}Pb . We aim for a modest value of the neutron skin thickness in ^{208}Pb of about $R_n - R_p = 0.16 \text{ fm}$. This value, although smaller as compared to other relativistic mean field models, is close to those predicted by many non-relativistic models. Note that when we change Λ_v , we also change g_ρ in order to maintain the symmetry energy fixed at $\sim 26 \text{ MeV}$ at a Fermi momentum of $k_F = 1.15 \text{ fm}^{-1}$. This procedure and the justification for it are described in detail in Ref. [3]. Increasing Λ_v in this fashion reduces the density dependence of the symmetry energy. This generates a symmetry energy at low densities

Model	$\rho_0 (\text{fm}^{-3})$	$\varepsilon_0 (\text{MeV})$	$K_0 (\text{MeV})$	$J (\text{MeV})$	$L (\text{MeV})$
NL3	0.148	-16.24	271.5	37.29	118.2
FSU	0.148	-16.30	230.0	32.59	60.5
IU-FSU	0.155	-16.40	231.2	31.30	47.2

TABLE II: Bulk parameters characterizing the behavior of infinite nuclear matter at saturation density ρ_0 . The quantities ε_0 and K_0 represent the binding energy per nucleon and incompressibility coefficient of symmetric nuclear matter, whereas J and L represent the energy and slope of the symmetry energy at saturation density.

that is *larger* than the one for FSU. As a result, protons near the surface of ^{208}Pb are pulled closer to the neutrons in an effort to minimize the neutron-proton asymmetry. This leads to an increase in the charge radius of ^{208}Pb . In order to maintain the charge radius in ^{208}Pb at its experimental value we must slightly increase the Fermi momentum of symmetric nuclear matter from 1.30 to 1.318 fm $^{-1}$. We then refit the parameters of the model to keep the other saturation properties of nuclear matter intact. Finally, the scalar coupling g_s is slightly tuned to improve the fit to the binding energies of closed shell nuclei. Note that we have not changed the scalar mass m_s from its FSU value.

The resulting parameter set—henceforth referred to as the *Indiana University-Florida State University (IU-FSU) interaction*—is listed in Table I. The resulting bulk properties of infinite nuclear matter have been collected in Table II. In addition, predictions for several ground-state properties of closed shell nuclei are listed in Table III and compared against other theoretical models and experiment (when available). Finally, predictions for the charge and neutron densities of ^{208}Pb are displayed in Fig. 1. Whereas significant differences can be observed in the prediction of the neutron densities, the difference among the models is small for the charge density. Note that although the parameters of the model will eventually be determined from an accurate calibration procedure, the new model reproduces rather well the charge radii and binding energies of closed shell nuclei. However, the IU-FSU interaction predicts the rather modest value of $R_n - R_p = 0.16$ fm for the, as yet unknown, neutron skin thickness in ^{208}Pb .

Nucleus	Observable	Experiment	NL3	FSU	IU-FSU
^{40}Ca	B/A (MeV)	8.55	8.54	8.54	8.53
	R_{ch} (fm)	3.45	3.46	3.42	3.41
	$R_n - R_p$ (fm)	—	-0.05	-0.05	-0.05
^{48}Ca	B/A (MeV)	8.67	8.64	8.58	8.55
	R_{ch} (fm)	3.45	3.46	3.45	3.44
	$R_n - R_p$ (fm)	—	0.23	0.20	0.17
^{90}Zr	B/A (MeV)	8.71	8.69	8.68	8.67
	R_{ch} (fm)	4.26	4.26	4.25	4.23
	$R_n - R_p$ (fm)	—	0.11	0.09	0.07
^{132}Sn	B/A (MeV)	8.36	8.37	8.34	8.33
	R_{ch} (fm)	—	4.70	4.71	4.68
	$R_n - R_p$ (fm)	—	0.35	0.27	0.22
^{208}Pb	B/A (MeV)	7.87	7.88	7.89	7.89
	R_{ch} (fm)	5.50	5.51	5.52	5.48
	$R_n - R_p$ (fm)	—	0.28	0.21	0.16

TABLE III: Experimental data for the binding energy per nucleon and charge radii for several doubly magic nuclei. Results are presented for the three models employed in the text alongside their predictions for the neutron skin thickness of these nuclei.

III. GIANT RESONANCES

At the time that the FSU effective interaction was calibrated, the only evidence in favor of a symmetry energy softer than NL3 came from nuclear collective excitations, particularly the mass dependence of the isoscalar giant monopole resonance (GMR). Whereas NL3—with an incompressibility coefficient of $K = 271$ MeV—was able to reproduce the centroid energy of the GMR in ^{208}Pb , it overestimated the GMR in ^{90}Zr . It was later confirmed that the success of the NL3 interaction in reproducing the breathing mode in ^{208}Pb was accidental, as it resulted from a combination of both a stiff EOS for symmetric nuclear matter and a stiff symmetry energy [30]. Indeed, with a relatively large neutron-proton asymmetry of $\alpha \equiv (N - Z)/A = 0.212$, the GMR in ^{208}Pb probes the incompressibility of neutron-rich matter, rather than that of symmetric matter. Given that the incompressibility of neutron-rich matter softens with α [31], NL3 could reproduce the GMR in ^{208}Pb by cancelling its stiff incompressibility coefficient K with a correspondingly stiff symmetry energy. This cancellation, however, is incomplete in ^{90}Zr because its nucleon asymmetry is almost twice as small as that of ^{208}Pb . Thus, to develop the FSU effective interaction we used the GMR in ^{90}Zr , rather than in ^{208}Pb , to fix the incompressibility coefficient of symmetric nuclear matter. Having fixed K , we used the GMR—and the isovector giant dipole resonance (IVGDR)—in ^{208}Pb to constrain the density dependence of the symmetry energy [21]. As we shall see below (see Table IV), the newly proposed IU-FSU effective interaction continues to reproduce the centroid energy of these three modes.

The distribution of both isoscalar monopole and isovector dipole strength were computed in a relativistic random-phase approximation (RPA). The first step in calculating the RPA response is the computation of the mean-field ground state in a self-consistent mean-field approximation. Once self-consistency is achieved, three important pieces of information become available: (i) the single-particle energies of the occupied orbitals, (ii) their single-particle wave

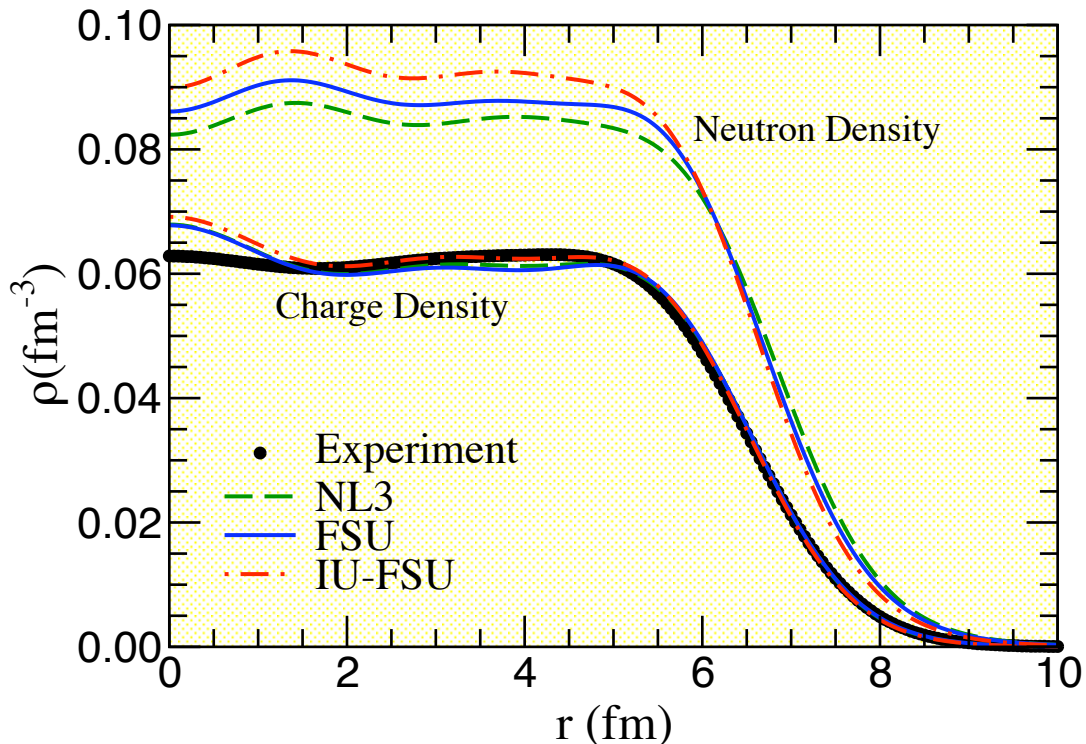


FIG. 1: (Color online) Model predictions for the charge and neutron densities of ^{208}Pb . The experimental charge density is from Ref. [29].

functions, and (iii) the self-consistent mean-field potential. This mean-field potential—without any modification—must then be used to generate the nucleon propagator; only then can one ensure the conservation of the vector current. The nucleon propagator, which is an essential building block of the uncorrelated polarization tensor, is computed non-spectrally to avoid any dependence on the artificial cutoffs and truncations that plague most spectral approaches. Moreover, a great merit of the non-spectral approach is that the continuum is treated exactly. Once the uncorrelated polarization insertion is computed, the correlated RPA polarization is obtained by iterating it to all orders with the consistent residual interaction. The distribution of strength is then obtained directly from the imaginary part of the polarization tensor. A detailed description of the relativistic RPA approach may be found in Ref. [26, 32]. Results for the centroid energies of the giant monopole and dipole resonances are presented in Table IV for the three effective interactions considered in the text. Unlike the NL3 model, the results obtained with both the FSU and the IU-FSU effective interactions are consistent with experiment.

Nucleus	Observable	Experiment	NL3	FSU	IU-FSU
^{208}Pb	GMR (MeV)	14.17 ± 0.28	14.32	14.04	14.17
^{90}Zr	GMR (MeV)	17.89 ± 0.20	18.62	17.98	17.87
^{208}Pb	IVGDR (MeV)	13.30 ± 0.10	12.70	13.07	13.24

TABLE IV: Centroid energies for the GMR in ^{208}Pb and ^{90}Zr , and the peak energy for the IVGDR in ^{208}Pb . Experimental data are extracted from Refs. [25] and [33].

IV. EQUATION OF STATE AND NEUTRON STAR STRUCTURE

Although the full complexity of the quantum system can not be tackled exactly, the energy density of asymmetric nuclear matter may be computed in a *mean-field* (MF) approximation. In the MF approximation all the meson fields are replaced by their classical expectation values and their solution can be readily obtained by solving the classical Euler-Lagrange equations of motion. The sole remnant of quantum behavior is in the treatment of the nucleon field which emerges from a solution to the Dirac equation in the presence of appropriate scalar and vector potentials [23, 34].

Following standard mean-field practices, the energy density of the system is given by the following expression:

$$\begin{aligned} \mathcal{E}(\rho, \alpha) = & \frac{1}{\pi^2} \int_0^{k_F^p} k^2 \sqrt{k^2 + M^{*2}} dk + \frac{1}{\pi^2} \int_0^{k_F^n} k^2 \sqrt{k^2 + M^{*2}} dk + \frac{1}{2} \left(\frac{m_s^2}{g_s^2} \right) \Phi_0^2 + \frac{\kappa}{6} \Phi_0^3 + \frac{\lambda}{24} \Phi_0^4 \\ & + \frac{1}{2} \left(\frac{m_v^2}{g_v^2} \right) W_0^2 + \frac{\zeta}{8} W_0^4 + \frac{1}{2} \left(\frac{m_\rho^2}{g_\rho^2} \right) B_0^2 + 3\Lambda_v W_0^2 B_0^2, \end{aligned} \quad (2)$$

where ρ is the baryon density of the system and $\alpha = (\rho_n - \rho_p)/\rho$ is the neutron-proton asymmetry. Alternatively, the energy density may be written in terms of the proton and neutron Fermi momenta k_F^p and k_F^n . Note that the following definitions have been introduced: $\Phi_0 \equiv g_s \phi_0$, $W_0 \equiv g_v V_0$, and $B_0 \equiv g_\rho b_0$. Also note that since the MF approximation is thermodynamically consistent, the pressure of the system (at zero temperature) may be obtained either from the energy-momentum tensor or from the energy density and its first derivative. That is,

$$P(\rho, \alpha) = \rho \frac{\partial \mathcal{E}}{\partial \rho} - \mathcal{E}. \quad (3)$$

The equation of state (pressure as a function of baryon density) for symmetric nuclear matter ($k_F^p = k_F^n$ and $B_0 \equiv 0$) is displayed in Fig 2. By design, the FSU and IU-FSU interactions have (almost) the same incompressibility coefficient so they predict similar pressures at low to intermediate densities. However, at higher densities the IU-FSU interaction is stiffer because it has a smaller value of ζ as compared to the FSU interaction. To date, the only terrestrial constraint on the high-density component of the EOS comes from energetic heavy-ion collisions. Both of these models predict equations of state that are consistent with the phenomenological flow analysis by Danielewicz, Lacey, and Lynch [15]. In contrast, the NL3 interaction, although enormously successful in reproducing ground-state properties of finite nuclei, predicts an equation of state that is significantly stiffer than the phenomenological extraction.

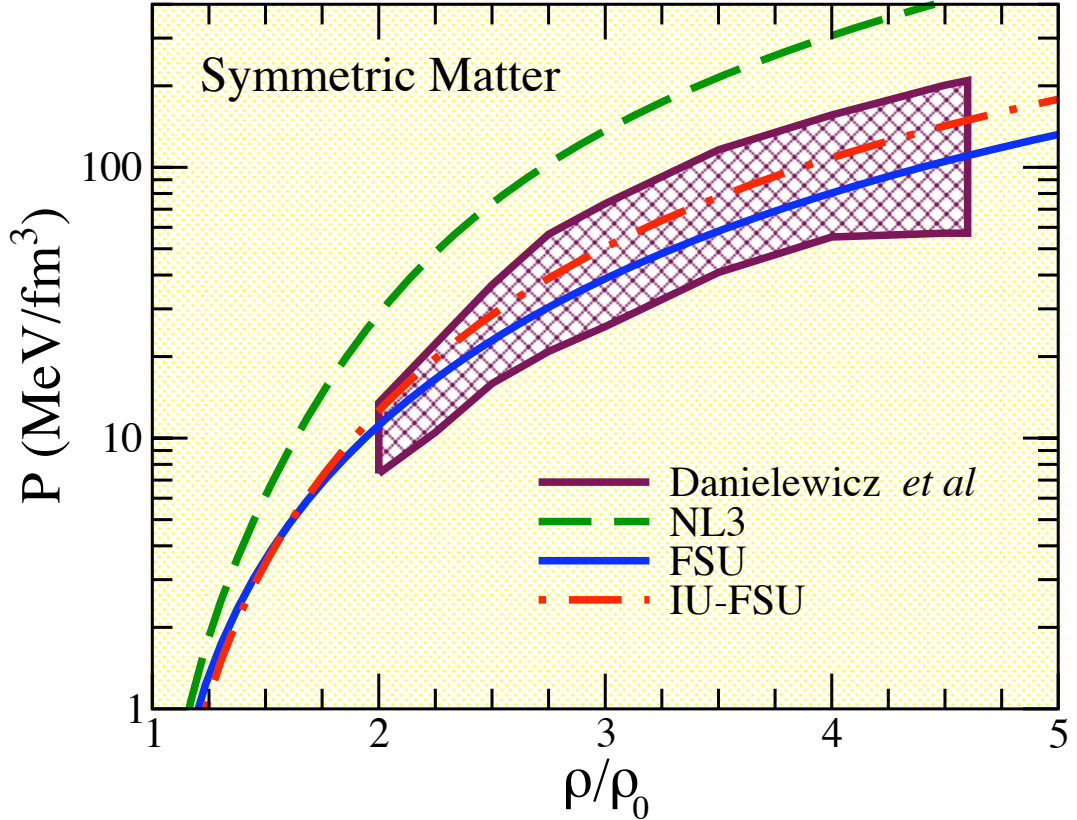


FIG. 2: (Color online) The equation of state—pressure P vs baryon density—of symmetric nuclear matter. Here ρ_0 is the density of nuclear matter at saturation and the shaded area represents the EOS extracted from the analysis of Ref. [15].

The equation of state of pure neutron matter (PNM) provides a powerful theoretical constraint on models of the effective interaction. By building on the universal behavior of dilute Fermi gases with an infinite scattering length,

significant progress has been made in constraining the equation of state of pure neutron matter [35]. To date, a variety of models using different neutron-neutron interactions and a variety of many-body techniques have been employed to compute the EOS of dilute neutron matter (see Ref. [36] and references therein). In Fig. 3 we display the energy per particle of pure neutron matter for a variety of microscopic approaches [36] and for the three relativistic effective interactions discussed in the text. In most relativistic descriptions the isovector interaction is modelled by the exchange of a single vector-isovector (“rho”) meson with its (Yukawa) coupling to the nucleon tuned to reproduce the symmetry energy at saturation density. Invariably, such a simple prescription generates a stiff symmetry energy. In turn, this yields an EOS for dilute neutron matter that is inconsistent with the model-independent results of Schwenk and Pethick (denoted by the shaded area in Fig. 3). The FSU isovector interaction improves on NL3 by adding an isoscalar-isovector mixing term (Λ_v) that softens the symmetry energy. Recall that such a softening is required to reproduce the centroid energies of various collective modes (see Table IV). Without any further adjustment, the FSU interaction is also consistent with the theoretical constraints (see solid blue line). Finally, the IU-FSU interaction—with an additional softening relative to FSU—remains within the theoretical “error bars”.

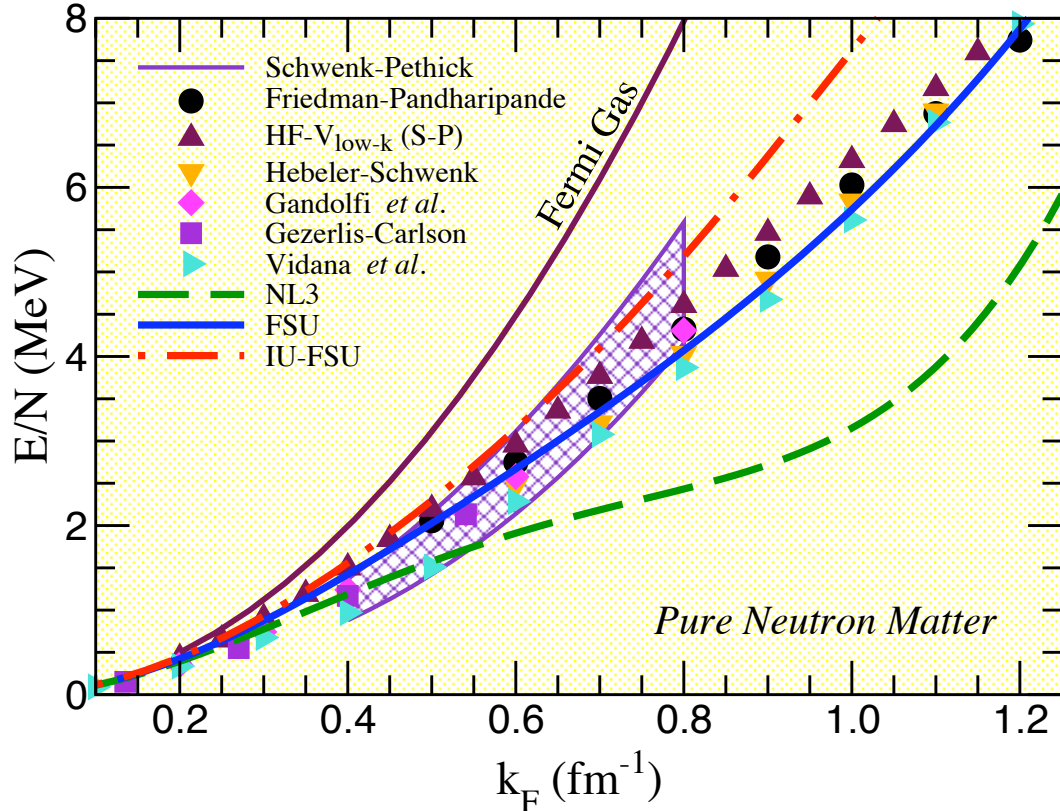


FIG. 3: (Color online) Energy per nucleon as a function of the Fermi momentum for pure neutron matter.

We conclude this section by computing the *mass-vs-radius* (M - R) relationship of neutron stars. Given that the structure of neutron stars is sensitive to the EOS over an enormous range of densities, we must resort to various descriptions. For the non-uniform outer crust we employ the equation of state of Baym, Pethick, and Sutherland [37]. At densities of about a third of nuclear-matter saturation density, uniformity in the system is restored. For this (liquid-core) region we use an EOS generated from the relativistic models discussed in the text. Although significant progress has been made in simulating the exotic structure of the inner crust (*i.e.*, the region between the outer crust and the liquid core) a detailed equation of state is still missing in this region. Hence, we resort to a fairly accurate polytropic EOS to interpolate between the solid crust and the uniform liquid core [38, 39]. The transition from the uniform liquid core to the solid crust is sensitive to the density dependence of the symmetry energy. The crust-to-core transition density ρ_t is obtained from an RPA stability analysis to determine the onset of the instability to small amplitude density oscillations [39]. With such an equation of state in hand, we can now proceed to integrate the Tolman-Oppenheimer-Volkoff equations to determine the structure of neutron stars.

In Fig. 4 we display predictions for the equation of state of stellar matter (*i.e.*, neutron-rich matter in beta equilibrium) for the three models discussed in the text, alongside the constraint extracted from Ref. [17]. For reference, also shown is the stiffest ($P = \mathcal{E}$) possible equation of state consistent with causality. As suggested in Ref. [17], the

FSU interaction appears slightly stiff at intermediate densities and too soft at high densities. The IU-FSU interaction successfully corrects both of these problems. Note, however, that the observational EOS can accommodate even stiffer equations of state. We stress that, if required, this can be implemented rather easily by reducing even further the value of ζ .

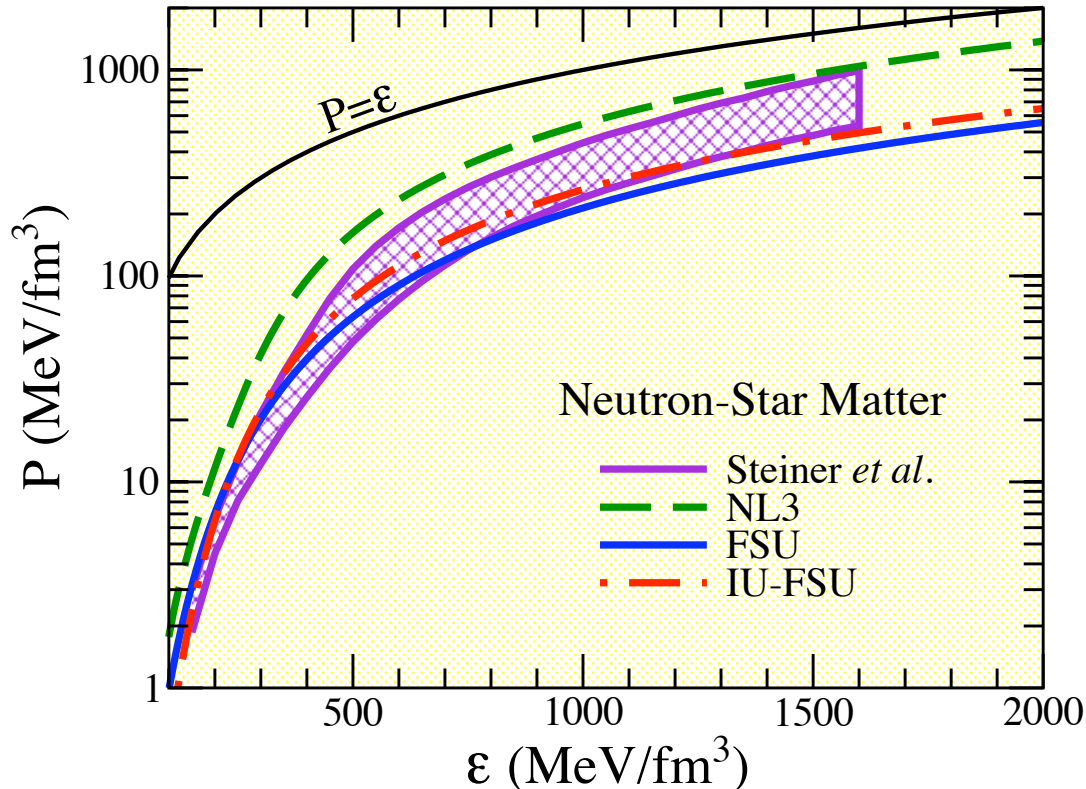


FIG. 4: (Color online) Equation of state—pressure vs energy density—of neutron-rich matter in beta equilibrium. The shaded region displays the observational constraint extracted from Ref. [17]. The solid black line ($P=\epsilon$) denotes the stiffest possible equation of state consistent with causality.

In Fig. 5 we display predictions for the M - R relation and compare them against observational constraints extracted from the analyses of Refs. [16] and [17]. The very stiff behavior of the EOS predicted by NL3 is immediately ruled out by both observational constraints. In the case of the FSU effective interaction, we recently identified a conflict when compared with the analysis by Ozel and collaborators [40]. Whereas the FSU model seems to generate an EOS that is consistent with observation, the predicted stellar radii were simply too large. Relative to the analysis by Steiner, Lattimer, and Brown [17], the FSU predictions overestimate the stellar radius—although not as much as suggested by [16]—but underestimates the maximum neutron star mass. The IU-FSU interaction, with a softer EOS at intermediate densities and a stiffer one at high densities, is motivated in response to these findings. Indeed, the IU-FSU interaction predicts a maximum stellar mass of $1.94 M_{\odot}$ and a stellar radius of $R = 12.49$ km for a $1.4 M_{\odot}$ neutron star (see Table V). These predictions are consistent with the 2σ values extracted from X-ray observations by Steiner, Lattimer, and Brown [17]. However, they are well outside the limits extracted by Ozel and collaborators [16]. Given that such extractions depend critically on the models used to simulate X-ray bursts, much work remains to be done to reconcile these two analyses. We close this section by listing in Table V predictions for several important neutron-star properties. In addition to the properties already discussed (such as masses and radii), the table includes the minimum density required for the onset of the direct Urca process and the minimum stellar mass that may cool down by the direct Urca process. Note that small neutron star radii and enhanced cooling are generally regarded as good indicators of a possible phase transition in the stellar core.

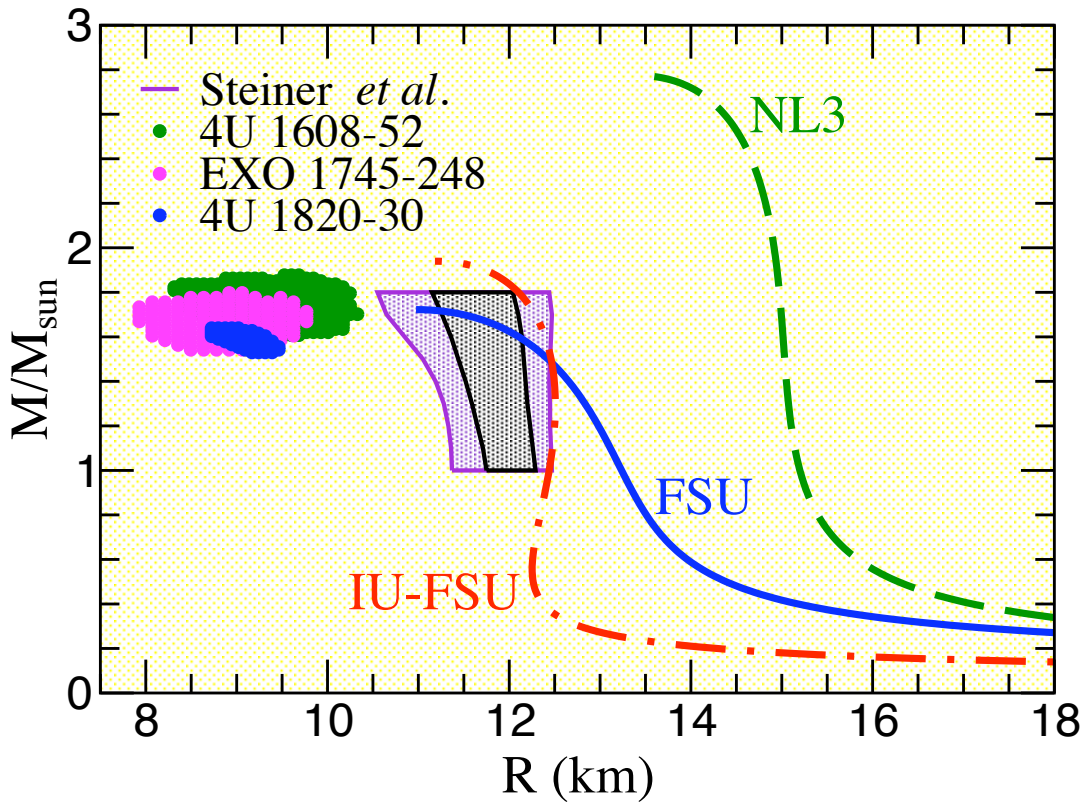


FIG. 5: (Color online) *Mass-vs-Radius* relation predicted by the three relativistic mean-field models discussed in the text. The observational data that suggest very small stellar radii represent 1σ confidence contours for the three neutron stars reported in Ref. [16]. The two shaded areas that suggest larger radii are 1σ and 2σ contours extracted from the analysis of Ref. [17].

Observable	NL3	FSU	IU-FSU
ρ_t (fm $^{-3}$)	0.052	0.076	0.087
R (km)	15.05	12.66	12.49
$M_{\text{max}}(M_{\odot})$	2.78	1.72	1.94
ρ_{Urca} (fm $^{-3}$)	0.21	0.47	0.61
$M_{\text{Urca}}(M_{\odot})$	0.84	1.30	1.77

TABLE V: Predictions for a few neutron-star observables. The various quantities are as follows: ρ_t is the transition density from non-uniform to uniform neutron-rich matter, R is the radius of a 1.4 solar-mass neutron star, M_{max} is the maximum mass, ρ_{Urca} is the threshold density for the direct Urca process, and M_{Urca} is the minimum mass neutron star that may cool down by the direct Urca process.

V. CONCLUSIONS

The structure of neutron stars depends sensitively on the equation of state of neutron-rich matter in beta equilibrium. As such, nuclear effective interactions play a critical role in astrophysical applications. Given the large extrapolations in isospin and density that are required to compute the EOS, it is imperative to constrain the effective interaction. Motivated by two recent analyses that have provided simultaneous mass and radius information on neutron stars [16, 17], we have introduced a new effective interaction constrained by the ground state properties of finite nuclei, their collective excitations, the properties of both dilute and dense matter, and the structure of neutron stars. Thus, experimental, theoretical, and observational constraints have all been incorporated into the calibration procedure.

Following the conclusions of Ref. [17]—that suggest that the accurately calibrated FSU effective interaction is slightly stiff at intermediate densities but soft at high densities—we have used two empirical parameters to correct these shortcomings. The new effective interaction—dubbed “IU-FSU”—softens the EOS at intermediate densities by reducing the neutron skin thickness of ^{208}Pb and stiffens the EOS at high density by increasing the maximum neutron star mass relative to the FSU predictions.

Existing relativistic mean-field interactions are flexible enough to reproduce, not only the charge density and binding

energy of closed shell nuclei, but also the neutron skin thickness of ^{208}Pb and the maximum neutron star mass [40, 41]. In particular, the density dependence of the symmetry energy is highly sensitive to the empirical parameter Λ_v . Thus, an increase in the value of Λ_v softens the EOS at intermediate densities and generates a neutron skin thickness in ^{208}Pb of only $R_n - R_p = 0.16$ fm. For comparison, the NL3 and FSU effective interactions predict significantly larger neutron skins: 0.28 fm and 0.21 fm, respectively. To stiffen the EOS at high densities we rely on the empirical parameter ζ [22, 40, 41]. Including ζ may be used to change the maximum neutron star mass by almost one solar mass without adversely affecting the bulk properties of nuclear matter around saturation density. Relative to the FSU model, the new IU-FSU interaction increases the maximum neutron star mass from $1.72 M_\odot$ to $1.94 M_\odot$.

As more accurate data becomes available, the coupling constants of the theory may need to be re-adjusted. The calibration procedure outlined here can accomplish this task rapidly and efficiently. Ultimately, however, one would rely on an *accurately* calibration procedure to determine the best-fit parameters of the theory and to obtain correlations among the various observables. Nevertheless, as it stands now the new IU-FSU relativistic effective interaction reproduces: (a) the binding energies and charge radii of closed-shell nuclei, (b) various nuclear giant (monopole and dipole) resonances, (c) the low-density behavior of pure neutron matter, (d) the high-density behavior of symmetric nuclear matter, and (e) the mass-radius relation of neutron stars. In the future, we plan to use the IU-FSU interaction to generate a finite-temperature/finite-density equation of state for use in supernova and neutron-star merger simulations [42, 43].

This work was supported in part by DOE grants DE-FG02-87ER40365 and DE-FG05-92ER40750.

-
- [1] B. A. Brown, Phys. Rev. Lett. **85**, 5296 (2000).
 - [2] R. J. Furnstahl, Nucl. Phys. **A706**, 85 (2002).
 - [3] C. J. Horowitz and J. Piekarewicz, Phys. Rev. Lett. **86**, 5647 (2001).
 - [4] C. J. Horowitz and J. Piekarewicz, Phys. Rev. **C64**, 062802 (2001).
 - [5] C. J. Horowitz and J. Piekarewicz, Phys. Rev. **C66**, 055803 (2002).
 - [6] A. W. Steiner, M. Prakash, J. M. Lattimer, and P. J. Ellis, Phys. Rept. **411**, 325 (2005).
 - [7] B.-A. Li and A. W. Steiner, Phys. Lett. **B642**, 436 (2006).
 - [8] J. M. Lattimer and M. Prakash, Phys. Rept. **442**, 109 (2007).
 - [9] K. Kumar, R. Michaels, P. A. Souder, and G. M. Urciuoli (2005), URL <http://hallaweb.jlab.org/parity/prex>.
 - [10] C. J. Horowitz, S. J. Pollock, P. A. Souder, and R. Michaels, Phys. Rev. **C63**, 025501 (2001).
 - [11] P. C. C. Freire, AIP Conf. Proc. **983**, 459 (2008).
 - [12] M. B. Tsang et al., Phys. Rev. Lett. **92**, 062701 (2004).
 - [13] M. B. Tsang et al., Phys. Rev. Lett. **102**, 122701 (2009).
 - [14] D. V. Shetty, S. J. Yennello, and G. A. Souliotis, Phys. Rev. **C75**, 034602 (2007).
 - [15] P. Danielewicz, R. Lacey, and W. G. Lynch, Science **298**, 1592 (2002).
 - [16] F. Ozel, G. Baym, and T. Guver (2010), 1002.3153.
 - [17] A. W. Steiner, J. M. Lattimer, and E. F. Brown (2010), 1005.0811.
 - [18] V. Suleimanov, A. Y. Potekhin, and K. Werner, Adv. Space Res. **45**, 92 (2010).
 - [19] G. A. Lalazissis, J. König, and P. Ring, Phys. Rev. **C55**, 540 (1997).
 - [20] G. A. Lalazissis, S. Raman, and P. Ring, At. Data Nucl. Data Tables **71**, 1 (1999).
 - [21] B. G. Todd-Rutel and J. Piekarewicz, Phys. Rev. Lett. **95**, 122501 (2005).
 - [22] H. Mueller and B. D. Serot, Nucl. Phys. **A606**, 508 (1996).
 - [23] B. D. Serot and J. D. Walecka, Adv. Nucl. Phys. **16**, 1 (1986).
 - [24] J. D. Walecka, Annals Phys. **83**, 491 (1974).
 - [25] D. H. Youngblood, H. L. Clark, and Y.-W. Lui, Phys. Rev. Lett. **82**, 691 (1999).
 - [26] J. Piekarewicz, Phys. Rev. **C64**, 024307 (2001).
 - [27] J. Piekarewicz, Phys. Rev. **C66**, 034305 (2002).
 - [28] G. Colò, N. Van Giai, J. Meyer, K. Bennaceur, and P. Bonche, Phys. Rev. **C70**, 024307 (2004).
 - [29] H. De Vries, C. W. De Jager, and C. De Vries, Atom. Data Nucl. Data Tabl. **36**, 495 (1987).
 - [30] J. Piekarewicz, Phys. Rev. **C69**, 041301 (2004).
 - [31] J. Piekarewicz and M. Centelles, Phys. Rev. **C79**, 054311 (2009).
 - [32] J. Piekarewicz, Phys. Rev. **C62**, 051304 (2000).
 - [33] J. Ritman and *et al.*, Phys. Rev. Lett. **70**, 533 (1993).
 - [34] B. D. Serot and J. D. Walecka, Int. J. Mod. Phys. **E6**, 515 (1997).
 - [35] A. Schwenk and C. J. Pethick, Phys. Rev. Lett. **95**, 160401 (2005).
 - [36] A. Gezerlis and J. Carlson, Phys. Rev. **C81**, 025803 (2010).
 - [37] G. Baym, C. Pethick, and P. Sutherland, Astrophys. J. **170**, 299 (1971).
 - [38] B. Link, R. I. Epstein, and J. M. Lattimer, Phys. Rev. Lett. **83**, 3362 (1999).
 - [39] J. Carriere, C. J. Horowitz, and J. Piekarewicz, Astrophys. J. **593**, 463 (2003).

- [40] F. J. Fattoyev and J. Piekarewicz, Phys. Rev. **C82**, 025805 (2010).
- [41] F. J. Fattoyev and J. Piekarewicz (2010), 1006.3758.
- [42] G. Shen, C. J. Horowitz, and S. Teige, Phys. Rev. **C82**, 015806 (2010).
- [43] G. Shen, C. J. Horowitz, and S. Teige (2010), 1006.0489.